Coupling between creep and redox behavior in nickel - yttria stabilized zirconia observed in-situ by monochromatic neutron imaging

Makowska, Malgorzata Grazyna; Kuhn, Luise Theil; Frandsen, Henrik Lund; Lauridsen, Erik Mejdal; De Angelis, Salvatore; Cleemann, Lars Nilausen; Morgano, Manuel; Trtik, Pavel; Strobl, Markus

Published in:
Journal of Power Sources

Link to article, DOI:
10.1016/j.jpowsour.2016.11.059

Publication date:
2017

Document Version
Peer reviewed version

Coupling between Creep and Redox Behavior in Nickel - Yttria Stabilized Zirconia Observed In-Situ by Monochromatic Neutron Imaging

Malgorzata Grazyna Makowska[1, 2], *Luise Theil Kuhn*[1], *Henrik Lund Frandsen*[1], *Erik Mejdal Lauridsen*[3], , *Salvatore De Angelis*[1], *Lars Nilausen Cleemann*[1], *Manuel Morgano*[4], *Pavel Trtik*[4], *Markus Strobl*[2]

[1] Technical University of Denmark, Frederiksborgvej 399, DK - 4000 Roskilde, Denmark
[2] European Spallation Source ESS AB, P.O Box 176, SE-221 00 Lund, Sweden
[3] Xnovo Technology Aps, Galoche Allé 15, DK-4600 Køge, Denmark
[4] Paul Scherrer Institut, CH-5232 Villigen PSI, Switzerland

Abstract: Ni-YSZ (nickel - yttria stabilized zirconia) is a material widely used for electrodes and supports in solid oxide electrochemical cells. The mechanical and electrochemical performance of these layers, and thus the whole cell, depends on their microstructure. During the initial operation of a cell, NiO is reduced to Ni. When this process is conducted under external load, like also present in a stack assembly, significant deformations of NiO/Ni-YSZ composite samples are observed. The observed creep is orders of magnitude larger than the one observed after reduction during operation. This phenomenon is referred to as accelerated creep and is expected to have a significant influence on the microstructure development and stress field present in the Ni-YSZ in solid oxide electrochemical cells (SOCs), which is highly important for the durability of the SOC. In this work we present energy selective neutron imaging studies of the accelerated creep phenomenon in Ni/NiO-YSZ composite during reduction and also during oxidation. This approach allowed us to observe the phase transition and the creep behavior simultaneously in-situ under SOC operation-like conditions.

Keywords: solid oxide cells, Ni-YSZ cermet, creep, neutron imaging

Abbreviations and symbols:

Ni/NiO-YSZ – nickel/nickel oxide - yttria stabilized zirconia
SOC - solid oxide electrochemical cell
SOFC - solid oxide fuel cells
SOEC - solid oxide electrolysis cells
SEM – scanning electron microscopy

*Corresponding author:
e-mail: malgorzata.makowska@frm2.tum.de
Address: Lichtenbergstr. 1, D-85747 Garching, Germany
Phone: +49 (0)89 289-14768

TGA – thermogravimetric analysis
TEM – tunneling electron microscope
CAHT-SPM - controlled atmosphere high-temperature scanning probe microscope
TOF - time of flight
BOA - Beamline for neutron Optics and other Application

I_n – normalized neutron beam intensity
I – neutron intensity transmitted through the sample
I_{OB} - open beam intensity
I_{DF} - dark field intensity
Σ – neutron macroscopic cross section

1. Introduction

Ni-YSZ (yttria stabilized zirconia) cermet has been widely used as fuel electrode in solid oxide cells (SOC) (both solid oxide fuel cells (SOFC) and solid oxide electrolysis cells (SOEC)) for efficient energy conversion of gas-to-power or vice versa during the past few decades and still remains one of the most popular materials for this application[1], [2]. Ni-YSZ layers for planar SOC are often produced by tape-casting and in such case they are prepared from a slurry containing NiO and YSZ, followed by sintering at high temperature (~1300°C), where metallic Ni is not stable. When fuel is supplied, NiO is reduced to Ni, making the material electrochemical active and more porous for enhanced gas transport. Microstructure of Ni-YSZ and in particular porosity, determines SOC performance [3]. Understanding of processes of reduction and re-oxidation of NiO/Ni-YSZ and the related microstructural and mechanical changes is crucial for designing efficient and durable cells and thus these processes have been widely investigated using a number of methods, among others SEM [4], [5], TGA[5], TEM[6], [7], CAHT-SPM (controlled atmosphere high-temperature scanning probe microscope)[8], impedance spectroscopy [9], [10], dilatometry [11].

If the oxygen partial pressure increases during utilization, nickel can oxidize and the consequent volume expansion can damage the microstructure of the electrode, the electrode support and the electrolyte in the cell [4], [12]. At the operating conditions, local increase of the oxygen partial pressure can occur for several reasons: sudden fuel supply interruption (while oxygen is still supplied through the electrolyte), air leakage (due to problems with sealing), high load

applied or high fuel utilization conditions (especially in case of high H_2O content in the fuel) or when no protective gas is used during shut down and start up [1], [12]. Therefore, redox cycling stability of Ni-YSZ electrodes is strongly desired.

Recent studies on the influence of stress on the reduction progress as well as the fact that SOC under real operating conditions are exposed to significant stresses have revealed the importance of investigating reduction and oxidation of NiO/Ni-YSZ under applied load, like it is the case during stack assembly and operation[13], [14]. It has been shown that there is a strong correlation between reduction progress and stress field development, which could also influence the phenomenon of accelerated creep in solid oxide fuel cell anode supports during reduction [15]. H. L. Frandsen et al. have observed significant deformations of NiO/Ni-YSZ composite samples during reduction conducted under external load. The observed deformations were orders of magnitude larger than the deformation observed due to the creep present when only load and temperature corresponding to operational conditions were applied. This phenomenon was explained by 1) softening and mobility of the NiO/Ni phase during the reduction process and 2) an associated release of residual stresses and 3) increased loading of the YSZ phase [15]. The total deformation was also explained to be due to a change of elastic stiffness during the reduction. This hypothesis is in good agreement with the results of the in-situ environmental TEM studies of NiO-YSZ reduction presented by S.B. Simonsen et al. in [6] who demonstrated a significant change of NiO/Ni particle shapes and positions during the reduction reaction. The accelerated creep is expected to have strong influence on the microstructure and stress field in Ni-YSZ cermet in SOCs, which are crucial for SOC performance and durability. Even though the effect of stress on the reduction of NiO-YSZ has been studied before, the recently demonstrated phenomenon of accelerated creep has shown that stress influence on the reduction process NiO-YSZ for SOC is not fully understood yet [15]. Hence, in-situ studies of this relation are important for the robustness of SOC stacks and should be considered in the further development of the technology.

In this paper, in-situ energy selective neutron imaging studies of the so called “accelerated creep” are presented. Neutron scattering techniques, in particular neutron diffraction has been applied to in situ studies of materials for SOFC anodes before [16], [17]. However, this method provides structural information on material, which is averaged over the whole measured volume. In contrast, energy selective neutron imaging holds a unique capability of simultaneous in-situ observation of deformation changes and phase transition with spatial and time resolution. Creep behavior and phase transition in NiO/Ni-YSZ composite were studied not only during reduction, but also during re-oxidation (redox cycling).

Energy resolved neutron imaging is based on the spatially and wavelength resolved measurement of the intensity of a neutron beam transmitted through the sample [18], which depends on various properties of the investigated material. For material characterization it is more convenient to convert measured intensity of the transmitted beam to the linear neutron attenuation coefficient, which is a material property, independent of the sample size. The linear attenuation coefficient, also referred to as total macroscopic neutron cross section, depends on the neutron wavelength. For polycrystalline materials, neutron transmission spectra contain so-called Bragg edges, which appear for neutron wavelengths equal to double the value of the lattice spacing ($2\ d_{hkl}$). Thus, measured patterns of the wavelength dependent attenuation coefficient contain information about the crystalline structure of the material and Bragg edge patterns can be used for qualitative and quantitative phase composition analysis. [19]–[22] Such measurements can be performed at both pulsed and continuous neutron sources [23], [24]. In the first case, pulses of neutrons with a broad wavelength spectrum are emitted from the neutron target and travel to the sample. Neutrons with different energies arrive at the sample and subsequently at the detector at different times called time of flight (TOF). More details about this approach can be found in [25]. The methodology and the specific principle of quantitative analysis of measurements on NiO/Ni-YSZ samples performed at pulsed neutron sources using the time-of-flight approach was described in previous work [26]. In contrast to the TOF method,

where the whole spectrum is acquired at once, energy selective imaging with a continuous beam must be performed by separate measurements at different neutron wavelengths selected by a monochromator or a velocity selector.

Here, the application of energy selective neutron imaging at a continuous neutron source for in-situ observations of phase composition changes in NiO/Ni-YSZ composite samples during reduction and redox cycling under external load is presented differing to previously demonstrated TOF approach. State-of-the-art short pulse neutron sources provide resolutions excessive for phase identification and quantification. Hence, a continuous monochromatic approach, where a relaxed wavelength resolution can be achieved, is currently more efficient for in-situ studies with high spatial resolution as required for this study because of higher neutron flux averaged over time. Correspondingly, also tomography resolving the phase composition of engineering materials in 3D has been enabled by a similar energy selective approach at a continuous source [22].

2. Experimental

1 mm thick plates of NiO-3YSZ anode support samples were prepared by hot pressing (200 kN applied for 1 min at 130 °C) of 5 layers (300 µm thick) of tape-casted layers. After hot pressing, the plate was cut into samples of dimensions 7 mm x 20 mm. The exact preparation procedure is described in a greater detail in [27].

For a number of 1 mm thick NiO-YSZ samples, consecutive reduction and oxidation processes were carried out during the neutron measurements at different temperatures and under different loads, using custom designed sample environment presented in [28]. This sample environment provides elevated temperature and atmospheres required for conducting reduction and oxidation, but also allows for applying stress to the samples. Moreover, for some samples several reduction – oxidation cycles were conducted. The samples and their treatment presented

in this work are summarized in Table 1. During the experiments, the samples were loaded by an applied dead-load (Figure 1). The stress field was modeled by a finite element analysis using the commercial software Comsol Multiphysics. The resulting stress field is illustrated in Figure 1 a), and the maximum stress is provided in Table 1.

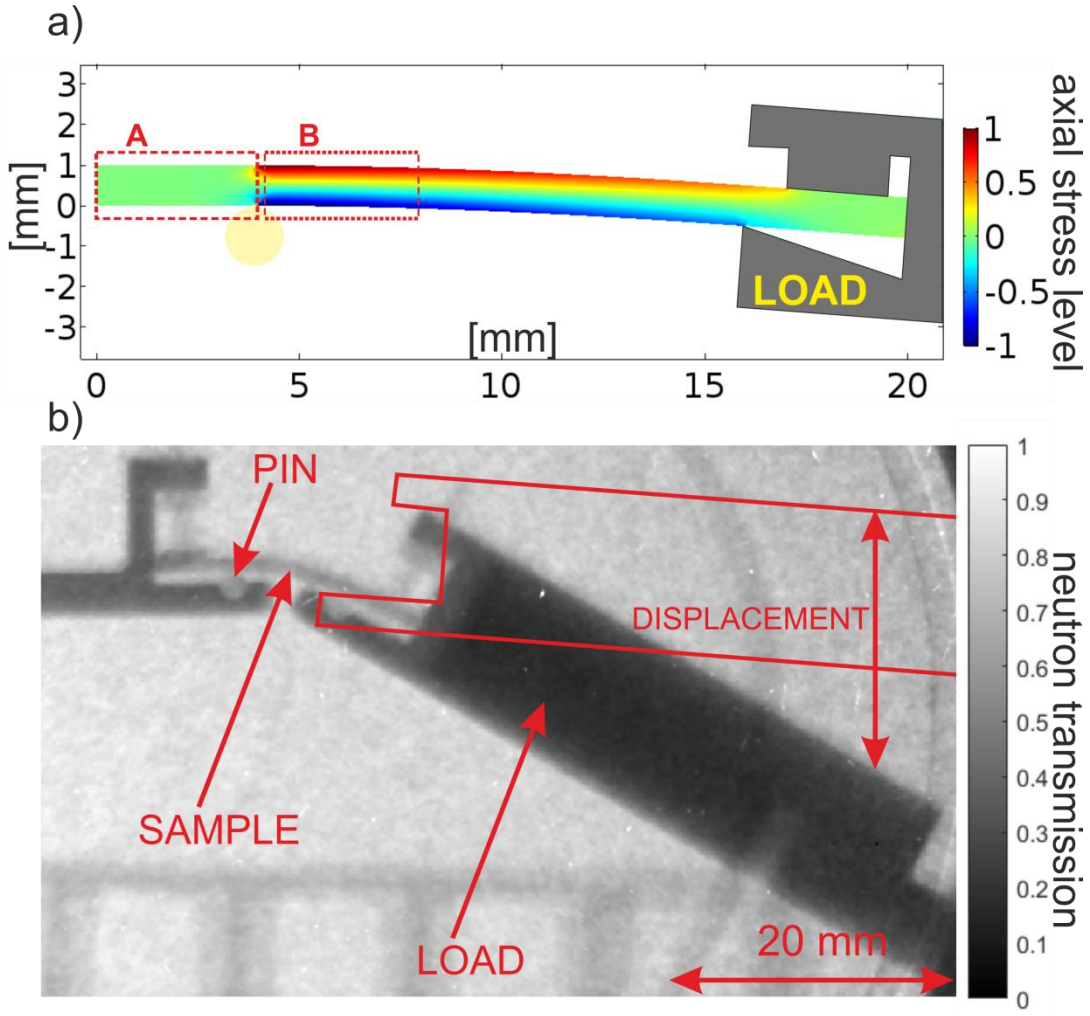

Figure 1. a) axial stress distribution in the sample due to the applied load evaluated using finite element analysis. Positive values on the color scale (normalized to the maximum) correspond to tension, and negative to compression; b) a neutron transmission image illustrating a deformation and the scheme for defining the load displacement.

Table 1. List of samples and their exposure to different temperatures, atmospheres, maximum axial stress due to the applied dead-load.

Sample	T [°C]	Reducing atmosphere [a)]	Oxidizing atmosphere	Processes sequence[b)]	Maximum stress[c)]
S1	650	9% H_2	None	R	-38 MPa / 29 MPa
S2	700	9% H_2	None	R	-38 MPa / 29 MPa
S3	800	9% H_2	None	R	-38 MPa / 29 MPa
S4	800	9% H_2	None	R	-82 MPa/64 MPa
S5	750	4% H_2	Air	R-OX-R-OX	-24 MPa / 19 MPa
S6	900	5% H_2	Air	R-OX-R-OX-R-OX-R-OX	-24 MPa / 19 MPa

[a)] (hydrogen concentration in inert gas); [b)] (R-reduction, OX-oxidation); [c)] (compression/ tension)

Both deformation and phase transition were observed in-situ during oxidation and reduction by means of monochromatic neutron imaging performed at the test Beamline for neutron Optics and other Application (BOA) at the Paul Scherrer Institute (PSI) [29].

Deformation of the samples due to the accelerated creep was observed in the time resolved series of neutron transmission images. As a measure of the deformation, the shift of the load fixed to the sample was used. The displacement of the load was defined as the relative vertical position change of the load from its initial position defined at the point indicated by the red arrow (DISPLACEMENT) in Figure 1 b) (48 mm from the fixed point in the sample, defined by the pin in the sample holder).

Phase transition was observed by local measurements and analyses of the neutron attenuation coefficient (macroscopic cross section), which, as was mentioned in the introduction, depends on the material composition and structure.

The neutron detection method utlilizes a neutron sensitive scintillator, which converts captured neutron radiation into photons of visible light, which consequently are recorded by a CCD camera [30], [31]. For this experiment a double crystal monochromator [32] and a detector setup consisting of a ^{6}Li-based scintillator and a CCD camera were utilized, resulting in an image with pixel size of 100 um. An extended Bragg edge pattern can be measured by a wavelength scan within a certain wavelength range, i.e. separate stepwise measurements at consecutive wavelengths with a defined step width. Taking into account the time needed for the acquisition of a single image (~ 60 s) and for changing the monochromator settings every time the wavelength is changed, measurement of this type require a time scale which is significantly longer than the time resolution meaningful for full pattern in-situ investigations and, in particular, for the process investigated here (up to 5 min).

Therefore, in order to achieve the required time resolution, in-situ neutron imaging measurements were performed with a single wavelength. For this purpose, first, the corresponding Bragg edge patterns were fully scanned for a wavelength range of 2.5Å to 4.5Å with a step of 0.05Å, before, during and after reduction using the so-called "stop-and-go" approach, which was described in detail in [33]. This kind of measurement is based on alternating steps of short-term chemical reaction phases, leading to increasing sample partial reduction and extended times of neutron image acquisition between each partial reduction. During the exposure the reduction process is stopped through changing the atmosphere to nitrogen and rapid cooling of the sample to room temperature (cooling process was no longer than 2-3 min).). The result of this is shown in Figure 2, where the Bragg edge patterns are illustrated for the sample measured after different times of reduction conducted at 650 °C. Bragg edges corresponding to Ni, NiO and YSZ phases are marked in the graph and their positions are in good agreement with theoretical values [34], [35].

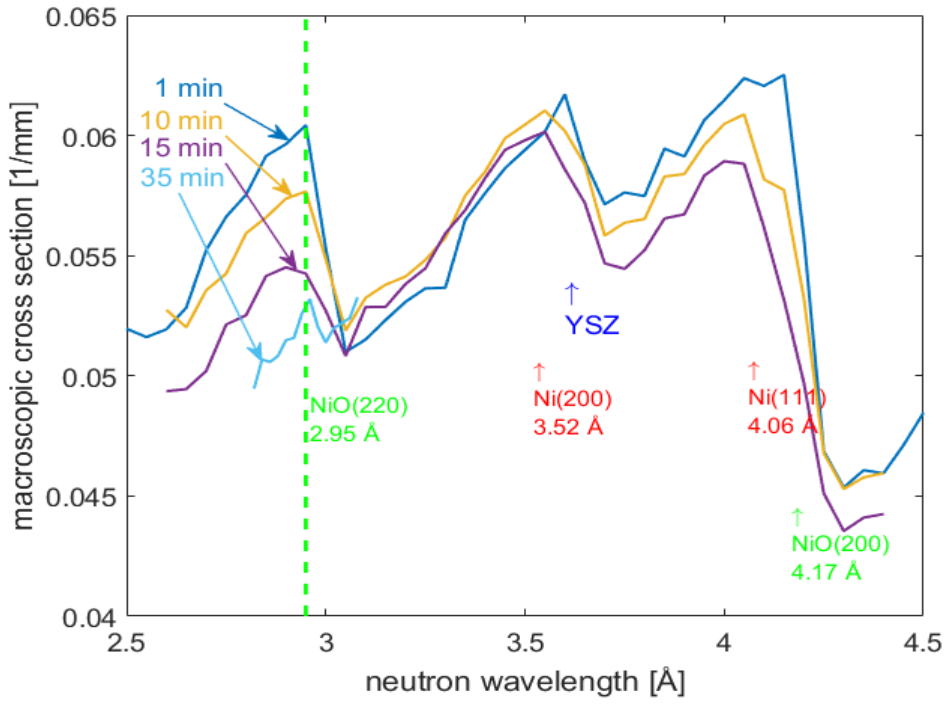

Figure 2. Bragg edge patterns of NiO-YSZ samples measured after 1, 10, 15 and 35 min of reduction at 650 °C.

Based on the results of these initial scans, a specific single wavelength, which correlates the most to changes of the reduction state, was chosen for the in-situ experiments. Consequently, all in-situ neutron imaging measurements were performed with a monochromatic neutron beam of wavelength 2.95Å, which is characteristic for the NiO Bragg edge corresponding to the (220) lattice planes. The chosen Bragg edge, which was marked with a green vertical line in Figure 2, is one of the most distinct edges in the attenuation spectrum of NiO/Ni-YSZ and, at the same time, it is well separated from the edges corresponding to any of the present phases (Ni, NiO or YSZ). In addition, the neutron spectrum utilized at BOA has its maximum value at around 3 Å, where hence the best flux conditions are provided.

The acquired images were normalized, according to the Equation (1).

$$I_n = \frac{I - I_{DF}}{I_{OB} - I_{DF}} \quad , \qquad (1)$$

where I_{OB} is the open beam intensity and I_{DF} for the dark field measuring the background and readout noise, when the beam shutter is closed. In order to enable analysis of the amount of NiO and Ni phases, the spatially resolved macroscopic cross section (Σ) was evaluated according to the Equation (2) (derived from the Beer-Lambert law):

$$\Sigma = \frac{1}{x} ln(I_n) \, , \qquad (2)$$

where x is the sample thickness (in beam direction). The macroscopic cross section is independent of the sample thickness, therefore it is more convenient for material characterization (in this case NiO and Ni phase content) than the measured intensity of the transmitted beam.

During the chemical processes (reduction and oxidation), changes of the Σ at the neutron wavelength of 2.95 Å (decrease and increase, respectively) were observed with spatial resolution. The measured value Σ, in contrast to the total value of the edge height (as can be

analyzed in full pattern measurements), depends not only on the phase content in the sample, but also on other material properties, such as the material density. As the density is subject to changes due to variations in porosity, different strain conditions throughout the sample and e.g. the evolution of cracks in the material, a straightforward accurate quantitative phase mapping is hindered in the case of pure monochromatic measurements. The macroscopic cross section is however still a good qualitative indicator of the composition of the NiO/Ni-YSZ samples.

After the in-situ neutron experiments, the resulting microstructure of selected samples was characterized by scanning electron microscopy (SEM), performed with a Hitachi TM3000 operated at 15 kV using the backscattered electron (BSE) detector. Images were quantified semi automatically by the mean linear intercept method, which allows for quantification of phase fractions and particle sizes from the images, using the program ManSeg v0.36© (in house developed by Jacob R. Bowen, DTU Energy).

3. Results and discussion

3.1. Creep during reduction

Figures 3 a-d present the local change of Σ at 2.95Å during reduction measured under applied load for two regions of the samples S1, S2, S3 and S4 at different temperatures (650 °C, 700 °C and 800 °C). The error of the measured data points was found to be on the order of 2% on average. The green and red lines correspond to the average Σ for sample regions A and B, respectively, which are defined in Figure 1 a). These represent a part of the sample with a low stress level (A) and a region with a high stress level (B). It is found that in each case the red curves corresponding to the sample part B, which is stressed the most, saturate faster than the green curves evaluated for sample part A. The saturation point corresponds to the end of the reduction process, as no more phase change and corresponding Σ change takes place afterwards. This confirms the results presented in [15], [33] indicating that the reduction rate is enhanced by stress in the material.

In the Ni/NiO-YSZ composite, YSZ phase acting as a backbone is chemically inert and the YSZ particles do not distort significantly if no external load is applied. During reduction of NiO particles, the oxygen atoms are removed from the material resulting in significant reduction of the volume of this phase [5], [11], [12]. Therefore, after reduction, spaces between the YSZ backbone particles in Ni-YSZ cermet are not completely filled, resulting in increased porosity. The growing porosity changes the density of the material, and hence it also has a significant influence on Σ (not only the phase change affecting the coherent elastic neutron scattering). When the material is completely reduced, pores can no longer be created, and also Bragg scattering is not changing anymore. Consequently, no change in the Σ is observed anymore and the curves in Figures 3 a-d reach their saturation at this point.

3.2. Effect of stress

The unstressed regions (green curves in Figure 3 a-d) reach significantly lower Σ values for the samples S2 (Figure 3 b), S3 and S4 (Figures 3 c and 3 d) reduced at 700 °C and 800 °C, respectively, compared to stressed regions (red curves). The Σ for the fully reduced samples must be the same for sample parts with the same material density. Thus, the difference in Σ in the completely reduced sample state can only be caused by differences in density (not by different phase content). Thus, the average density of the whole stressed part B appears to be higher as compared to the unstressed part A. It can be concluded that there are significant structural differences in the regions A and B, which could be due to higher porosity or significantly more cracks created in the unstressed region (A). However, during reduction (first reduction process from the sintered state), cracks are normally not observed.

In the region B, both tensile and compressive stresses are present on the top and bottom side of the sample respectively. The increased density in this region indicates that the effect of compression on the density is more significant than the one of tensile stress. This can be caused by two things:

- Maximum calculated stress on the compressed side is higher than on the top side exposed to tensile stress.
- Contraction of NiO particles during reduction normally leads to contraction of the composite and thus it can enhance the effect of compression. Hence, at the same time, it might also act against the effects of tensile stress.

Stress applied to the sample, which is concentrated in the region B, results in accelerated creep causing bending of the sample. Previously it was suggested that accelerated creep is caused by mobility of the NiO/Ni phase during the process [15]. Thus, from the microscopic point of view, the deformation of the loaded sample results in a change of the shapes and positions of the Ni/NiO particles and also in displacement of the YSZ backbone particles. Therefore, the distances between YSZ particles can increase in the material under tension and decrease in the material under compression. Consequently, the porosity on the compressed side is expected to be lower than on the side subjected to tensile stress, where the porosity might be increased, but according to our results not compensating the lower porosity on the compressed side.

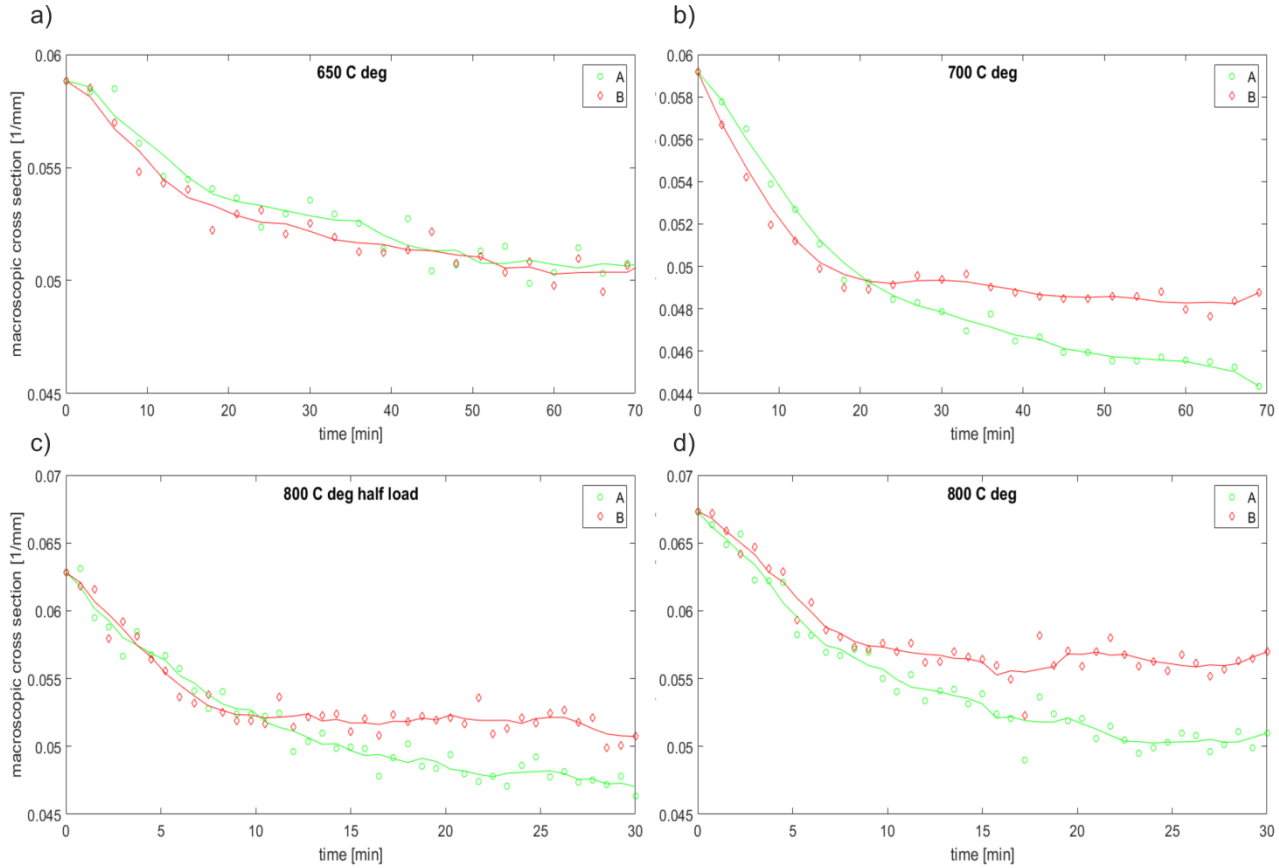

Figure 3. Macroscopic cross section of NiO-YSZ measured during reduction conducted at 650°C (a), 700°C (b) and 800◦C (c - lower load, d – higher load) under applied load (stress values are given in the table 1).The Green and red curves correspond to the sample regions A (low stress region) and B (high stress region), respectively, as illustrated in figure 1 a).

3.3. Effect of temperature

Reduction is faster at higher temperatures, which is observed by quicker saturation of the curves in Figure 3 at increased temperatures (note the different time-scale in Figure 3 c and d). While both reduction and density changes related to the accelerated creep affect the measured Σ, the effect of these two factors appears different at different temperatures. At lower temperatures, the accelerated creep is slower and the deformation obtained after full reduction is smaller than at higher temperatures. The accelerated creep takes place at any temperature as long as the temperature is high enough to initiate the reduction of NiO. However, the deformation due to accelerated creep, reached after total reduction or at a given reduction degree (e.g. for a sample reduced to 50 % of the initial NiO amount), depends strongly on the temperature. This can be related to the fact that, at lower temperatures (here meaning 650 °C -700 °C) Ni is significantly stiffer than at 900 °C making the deformation effect on the Σ more significant at higher

temperatures. Although the reduction rates depend on the temperature (it slows down significantly with decreasing temperature [33]), the same reduction state (complete reduction) could be reached at all temperatures in the considered range (650 °C -900 °C). Thus, under the assumption that the material density is not altered additionally, the final effect of reduction on Σ is independent of temperature i.e. a given reduction degree value e.g. 50% results always in the same change of Σ with respect to the initial 0% reduction degree, regardless of the reduction temperature. Changes of density, i.e. porosity, can only add to this effect, positively or negatively. Hence any deviation in the fully reduced state can be attributed to these structural effects.

Correspondingly in the case of reduction at 650 °C, when the deformation of the sample is very small the stressed and non-stressed parts of the sample (B and A, respectively) saturate at the same Σ value, as it can be seen in Figure 3 a.

A similar influence on Σ as by the temperature is observed with respect to the load. Increasing load also enhances deformation, affecting the material density, and thus its Σ. Such difference can be observed as shown in Figures 3 c and 3 d, which present the results for two samples S3 and S4, which were reduced at 800 °C, but with different load values.

3.4. Creep during redox cycling

3.4.1. Effect of level of partial oxygen pressure changes

In the next part of this study, the phase transition and creep in NiO/Ni-YSZ composite were observed during full redox cycles. First in-situ studies of redox cycling were performed switching the atmosphere between 9% hydrogen/91% nitrogen and air. Using this hydrogen concentration, the samples often broke during the treatment and it was difficult to conduct several redox cycles of the samples under load. The authors believe that the phenomenon of the accelerated creep can help to release the stresses occurring due to the phase transition in NiO/Ni-YSZ, but in some cases, this effect is not sufficient, or not sufficiently fast, resulting in

breaking of the samples. A lower hydrogen concentration slows down the reduction rate significantly, and it was observed that, for lower hydrogen concentration, sample failures were less frequent. Therefore, examples of two samples (Figures 4 and 5), which were reduced in atmospheres with hydrogen concentrations of 4% and 5%, are presented in this work.

3.4.2. Accelerated creep during oxidation

From Figures 4 and 5 it is clear that accelerated creep takes place not only during reduction of NiO-YSZ, but also during re-oxidation. This fact was observed for the first time during the neutron imaging measurements presented here. This phenomenon indicates that the NiO/Ni phase becomes mobile also during oxidation of the Ni particles.

Elastic stiffness of NiO is higher as compared to Ni. Moreover, the elastic stiffness decreases due to the change of porosity of the composite when NiO is reduced to Ni, which results in further deflection. An increase of the composite elastic stiffness can be expected during the oxidation, thus in this case the deflection cannot be explained partially by the drop of elastic stiffness as in [15]. The deflection in this case must thus purely be due to a 1) softening of the Ni phase and 2) primary creep of the YSZ phase.

The difference between the deformation rate and amount of deformation observed during the oxidation and reduction stages could be due to that in the case of oxidation, the structure is stiffened elastically and in the case of reduction the structure is softened elastically.

It is also evident that, the oxidation reaction is slower than the reduction process. During reduction the Σ values decrease very fast in the first minutes of the process, while the oxidation rate is more homogeneous during the whole process as indicated by the Σ behavior (Figures 4, 5). This could be due to that the structure is opening during reduction, while it is closing through oxidation. However the gas-diffusion in these structures is much faster than the reaction kinetics and diffusion in the solids. Therefore, this is most likely due to the faster oxygen diffusion in Ni compared to that in NiO. The oxidation rate depends, however, just like the reduction, on

the temperature and is significantly faster at 900 °C (sample S6, Figure 5) than at 750 °C (sample S5, Figure 4).

3.4.3. Correlation between accelerated creep and redox

Figure 4 a) presents the deformation of the sample S5 (Table 1) due to the accelerated creep occurring during two redox cycles performed at 750 °C under applied load. The deformation is measured by the position change of the load as outlined earlier. Figure 4 b) illustrates the Σ changes during the reduction and oxidation. From the comparison of the curves illustrating phase change and deformation, it can be noticed that the speed of the creep is proportional to the reaction rate, i.e. the load position changes faster, when the phase transition is faster; and slower, when the reaction slows down. It is also apparent that, when the Σ curves reach a plateau (meaning that the given chemical reaction is finished), no creep is observed anymore, even though all the externally applied conditions, i.e. temperature, atmosphere and load, remain unchanged.

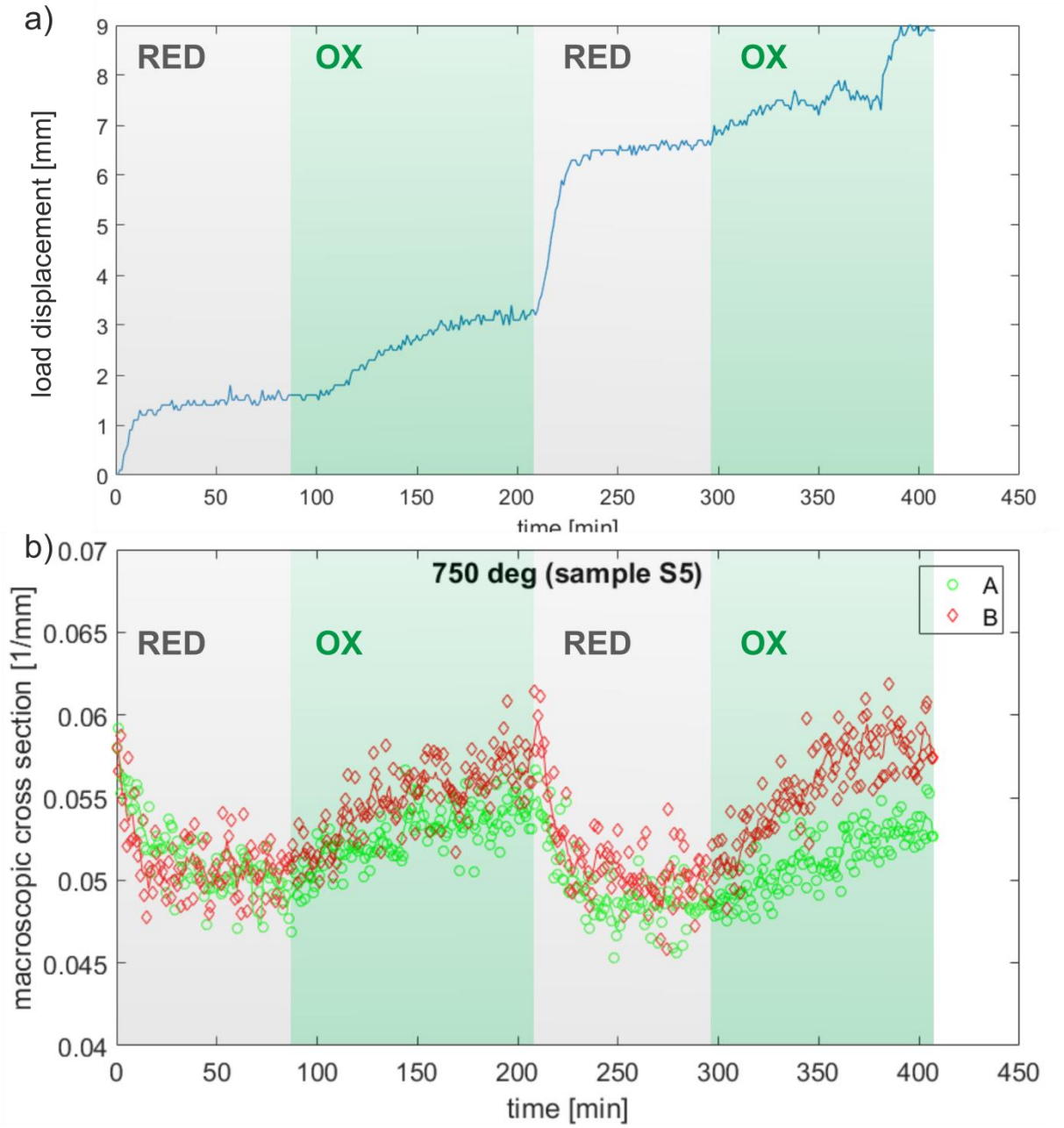

Figure 4. a) Displacement of the load on the NiO-YSZ sample S5 measured during redox cycles at 750°C loaded with half weight (with respect to the other samples). b) Macroscopic cross section of the sample; green and red curves correspond to the regions A (low stress region) and B (high stress region), respectively, as illustrated in figure 1 a).

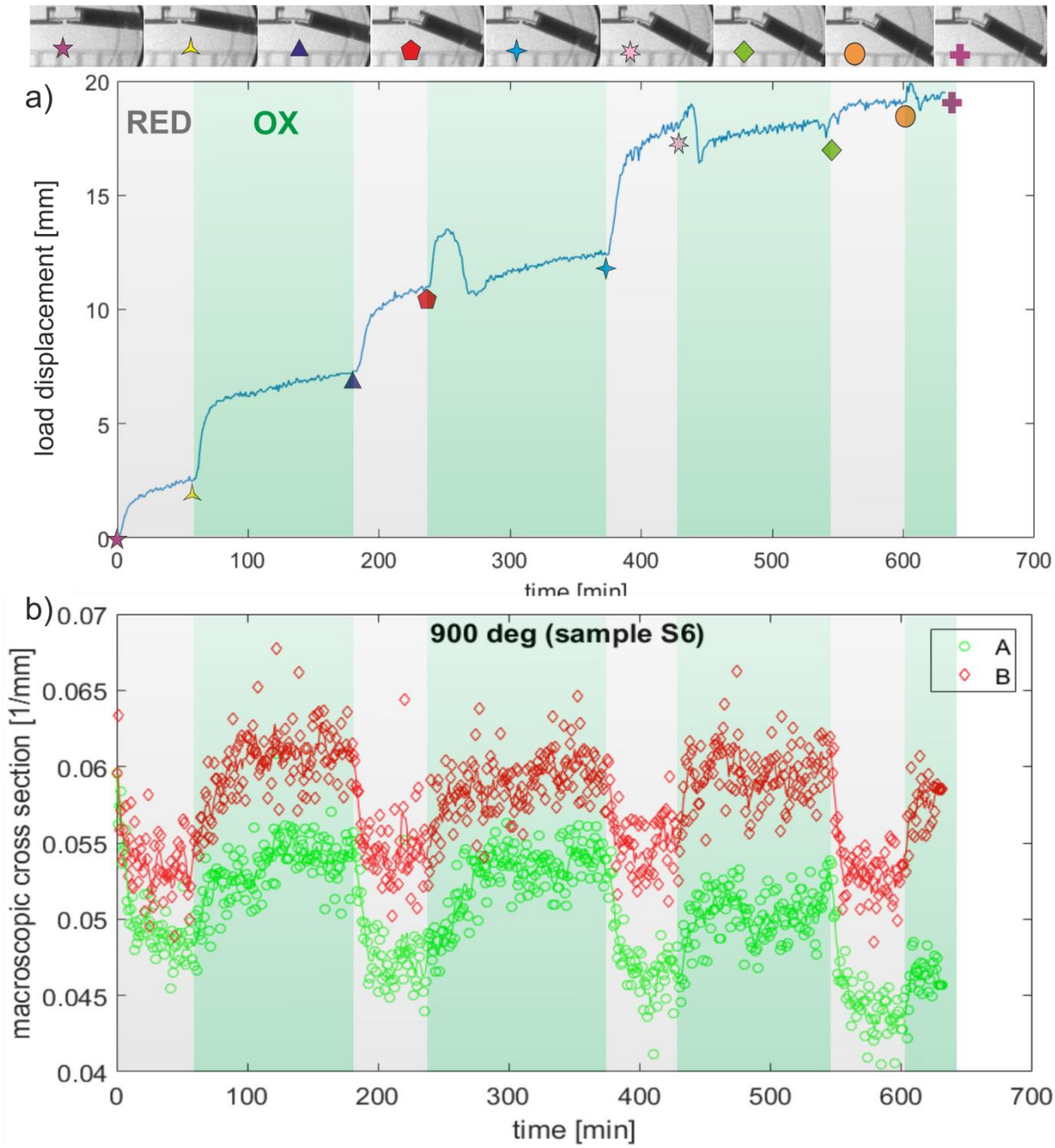

Figure 5. a) Displacement of the load on the NiO-YSZ sample S6 measured during redox cycles at 900°C loaded with half weight (with respect to the other samples). b) Macroscopic cross section of the sample; green and red curves correspond to the regions A (low stress region) and B (high stress region), respectively, as illustrated in figure 1 a).

3.4.4. Reduced damage in stressed parts during redox

Figure 5 a) presents the deformation of the sample S6 due to accelerated creep occurring during four redox cycles performed at 900 °C under applied load, and Figure 5 b) illustrates the Σ changes occurring during these processes.

In both Figures 4 and 5, growing difference between red and green curves during redox cycling can be observed. This discrepancy between attenuation coefficient Σ corresponding to the nonstressed and stressed regions A and B increases with each cycle and, as it is apparent for completely reduced and completely oxidized states, it must be related to a growing difference in microstructure in the two regions. Lower Σ values at completely reduced or oxidized states for region A with respect to region B indicate lower density, which can be related to higher porosity or other microstructural changes like cracks.

The SEM micrographs presented in Figure 6 show cross sections of the sample S6 in the regions A and B after the treatment. These micrographs reveal that in this case, the higher density in region B than in A is a result of more cracks appearing and growing during redox cycles in the unstressed region A. The same differences (more cracks in the region A) were observed in SEM images of the sample S5.

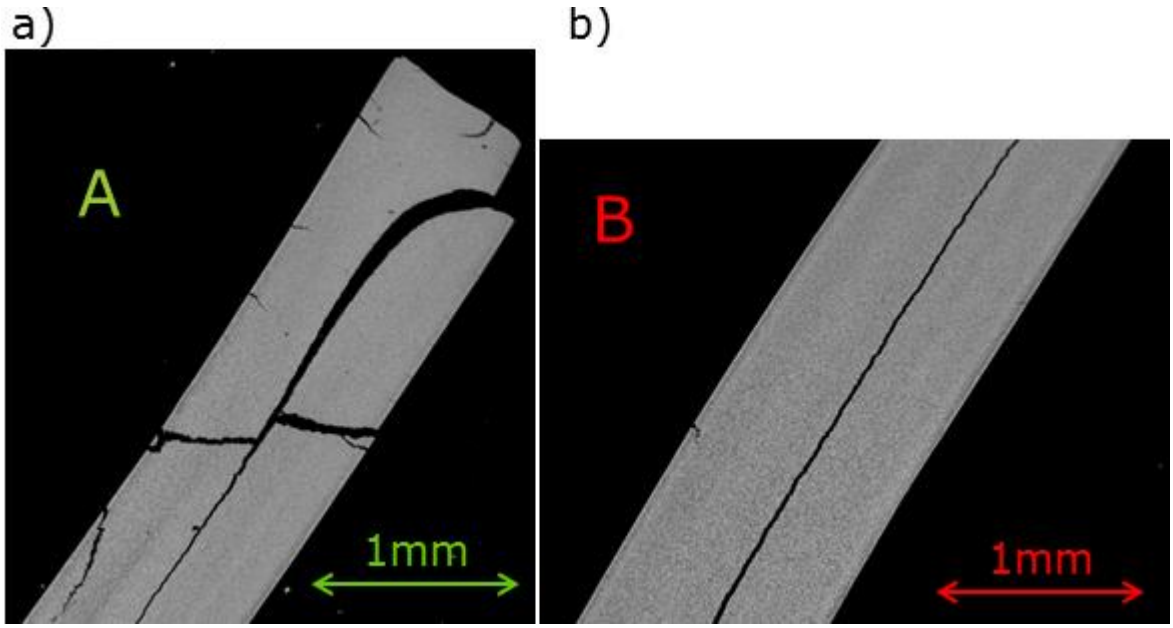

Figure 6. SEM images of a cross section of sample S6 of a) the region A and b) the region B (see figure 1 a)).

The reason might be that induced primary creep of the YSZ phase enables it to adapt better to the internally generated stress of the Ni phase expansion during oxidation. In the bottom part

of the sample the externally applied compressive stress could also prevent that the YSZ phase breaks apart, by counteracting the internally generated stress from the Ni phase expansion.

The appearing cracks apparently govern the long term decrease of the macroscopic cross section in region A. However, this decrease can be observed already during the first reduction process (also in case of samples S1-4 described in the previous section), during which cracks are generally not expected to appear. That means that cracks are not the only factor causing this density change. Moreover, in case of sample S6 the change appears mostly during reduction reactions (not oxidation), which supports the hypothesis (outlined in the section "Effect of stress") that increased density in region B is because during reduction, the effect of compression is more significant than the effect of tensile stress. Again, the higher the temperature, the lower is the stiffness of particular phases (especially Ni phase) and thus changes in microstructure are more significant.

3.4.5. Upwards deflection after multiple redox cycles

Most remarkably Figure 5 a) documents an upwards bending of the sample against gravity and load force during the second and the third oxidation reactions. The effect is especially distinct in the time period corresponding to the second oxidation process. After introducing air in the sample environment in the 240th minute of the process, both oxidation and creep started and resulted in moving the load initially downwards. However, after about 15 min of oxidation, the movement due to the creep has reversed its direction and the load started to move upwards.

The scheme presented in Figure 7 a) represents expected structural changes during consecutive reduction and oxidation reactions with and without load proposing a possible scenario compatible with the observations. The reduction of the material under tension results in increasing distances between YSZ particles (Figure 7 a) (4)) and in the compressed part of the material distances between YSZ particles decrease (Figure 7 a) (6)), while in the case without load relative positions of YSZ particles do not change (Figure 7 a) (3, 5)). Consequently, the

tensioned material part contains more voids than the compressed part. This discrepancy enhances with every consecutive redox cycle and finally, dense packing and low porosity on the compressed side (bottom side) and high porosity on the tensioned side (top side) are achieved.

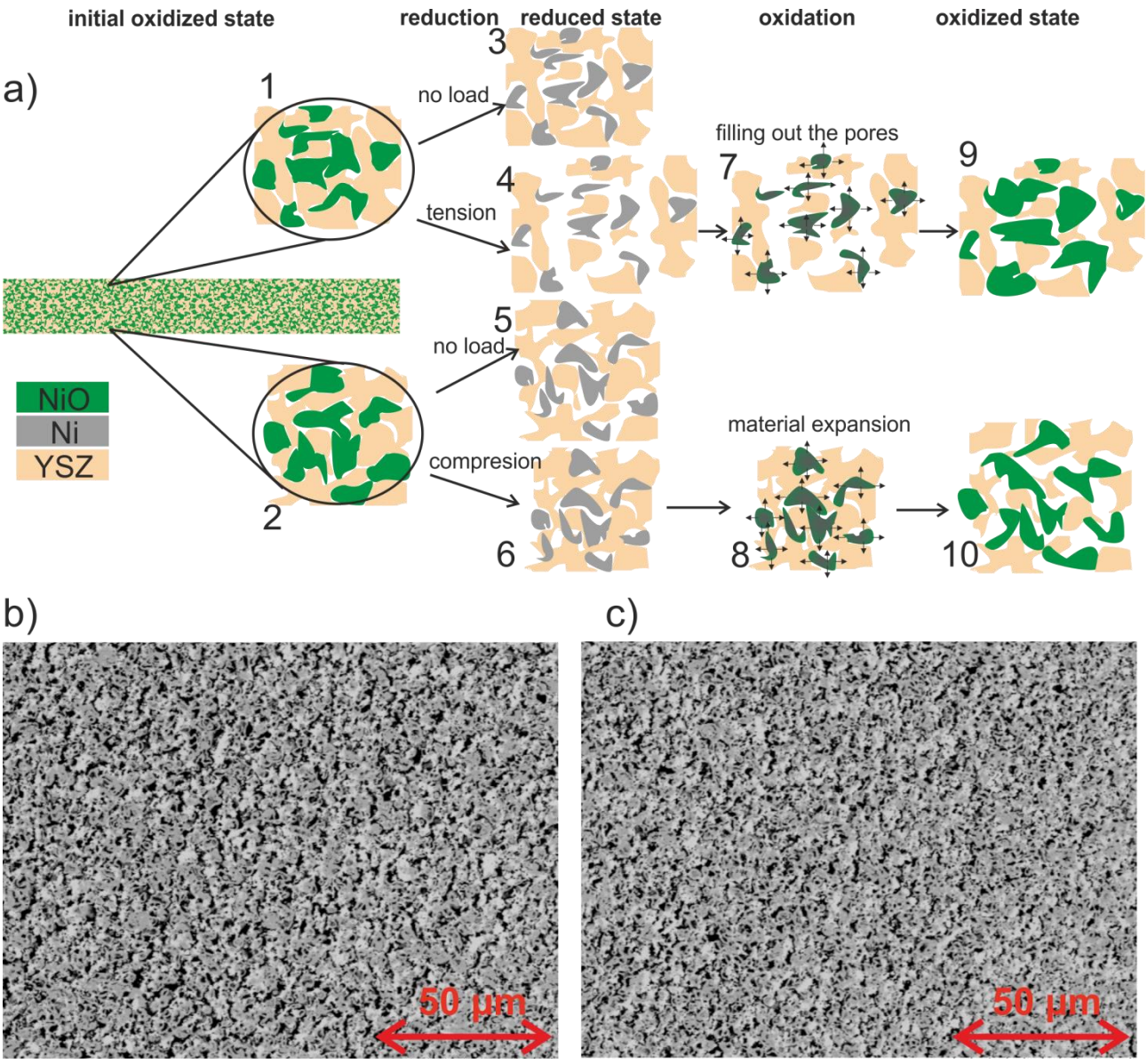

Figure 7. a) Structural changes in the NiO/Ni-YSZ composite during redox cycling with and without load (detailed description in text); SEM images of a cross section of sample S6 in the stressed region B of b) material under compression – bottom part and c) material under tensile stress – top side of the sample (see figure 1 a)).

During oxidation the Ni particles expand into positions similar to their original place from when they were sintered. However, due to the significant distortions of the samples achieved at

900 °C and consequently distortions of the microstructure, the space originally occupied by the NiO phase in the compressed (bottom) side has vanished significantly compared to the initial structure. Thus, expansion of Ni can only occur by increasing the volume of the composite (Figure 7 a) (8, 10)). On the tensile stressed side, the pores created during reduction have been opened more compared to the original microstructure, where these have been occupied by NiO, and thus the expansion of the Ni phase during oxidation does not induce a distortion, i.e. expansion of the material volume (Figure 7 a) (7, 9)). Therefore it is plausible that an expansion at the bottom side of the sample is suited to cause the observed upwards movement of the load attached to the sample. For simplicity, the scheme in Figure 7 a) presents situation, in which a sample bends upwards already during first oxidation. However in case of sample S6 it occurred during the second oxidation.

Figures 7 b,c) presents SEM micrographs of the sample S6 after treatment. Both images contain three phases: light gray illustrating YSZ, dark gray – NiO and black – pores. The fractions of porosity in the regions shown in Figures 7 b,c) were evaluated using the Mean Linear Intercept method, which allows for quantification of phase fractions and particle sizes from the images. Calculated porosity in the compressed region was 33(3)% and 37(3)% in the tensed part. This is in accordance with the conditions for the above outlined and illustrated (Figure 7 a)) hypothesis.

According to the stated hypothesis explaining the bending of the sample upwards against the applied load, the difference in porosity was expected to be especially significant in the reduced state. However such difference can be observed even in the oxidized state, which is illustrated in the presented SEM images, measured after all the conducted redox cycles i.e. at the oxidized state of the sample. Lower porosity on the compressed side of the sample observed even after oxidation is consistent with the stated hypothesis.

4. Conclusion

In this work the phenomenon of so-called accelerated creep of Ni(O)-YSZ solid oxide cell anodes has been studied in-situ through a combination of a phase transition and deformation observation by means of energy resolved neutron imaging. The phenomenon was studied during initial reduction, but also in reduction-oxidation (redox) cycles. Neutron imaging experiments were performed at BOA beamline at the continuous spallation neutron source SINQ at PSI. It was found that:

- phase changes can be observed in-situ at a continuous neutron source using a monochromatic beam.
- for the NiO to Ni phase change a wavelength of 2.95 Å corresponding to one of the NiO Bragg edges was found to provide the best contrast.
- neutron imaging can be utilized to also observe deformations and hence creep rates to further study the relationship between redox cycles and the "accelerated creep", which was previously demonstrated in NiO/Ni-YSZ samples during reduction.

By applying this method to study reduction and redox cycling processes in NiO/Ni-YSZ, it was found that:

- After reduction the more stressed regions are denser, less porous, than unstressed regions. It was assumed that the reason for this is that compressive creep is assisted by the contraction of the Ni phase during reduction, so effect of creep on the compressed side cannot be fully counterbalanced by the effect of creep on the tensile side.
- "Accelerated creep", observed before during the first reduction of NiO-YSZ layers, takes place also during re-oxidation as well as during further repeated consecutive reduction and oxidation treatments. This indicates that the primary creep of the YSZ is acting to a high degree in both reduction as well as oxidation processes.
- The deformations caused by the accelerated creep were, however, more significant during reduction. This could be due to elastic stiffening (stiffening related to both phase and porosity change) during oxidation and softening during reduction.

- The stressed regions display less damaged (less cracks) than the unstressed after redox cycling. The authors believe that the stress and resulting primary creep of the YSZ backbone facilitates adaption of two phases to each other. The damage was first observed during the in-situ experiments as more significant long term decrease in density in the unstressed regions as compared to the stressed regions. Consequent scanning electron microscopy confirmed that lower density in the unstressed region was caused by more cracks as compared to stressed region.

Measurements performed during several redox cycles have shown that density in the unstressed part of the sample after cycling becomes significantly lower than in the stressed part.

Acknowledgements
The authors are grateful to J. R. Bowen (jrbo@dtu.dk) for the availability of ManSeg v0.36 who's development was partially funded by the EU FP7 RELHY project (Grant Number: 213009). The authors wish to thank J. Johnson, J. E. Jørgensen and J. S. Andersen for help in designing and building the sample environment for presented experiments and DanScatt for financial support for neutron beam time travels.

[1] B. Shri Prakash, S. Senthil Kumar, and S. T. Aruna, "Properties and development of Ni/YSZ as an anode material in solid oxide fuel cell: A review," *Renew. Sustain. Energy Rev.*, vol. 36, pp. 149–179, Aug. 2014.

[2] N. Mahato, A. Banerjee, A. Gupta, S. Omar, and K. Balani, "Progress in material selection for solid oxide fuel cell technology: A review," *Prog. Mater. Sci.*, vol. 72, pp. 141–337, Jul. 2015.

[3] H. Shimada, T. Suzuki, T. Yamaguchi, H. Sumi, K. Hamamoto, and Y. Fujishiro, "Challenge for lowering concentration polarization in solid oxide fuel cells," *J. Power Sources*, vol. 302, pp. 53–60, 2016.

[4] J. Malzbender, E. Wessel, and R. Steinbrech, "Reduction and re-oxidation of anodes

for solid oxide fuel cells," *Solid State Ionics*, vol. 176, no. 29–30, pp. 2201–2203, Sep. 2005.

[5] S. Modena, S. Ceschini, A. Tomasi, D. Montinaro, and V. M. Sglavo, "Reduction and Reoxidation Processes of NiO/YSZ Composite for Solid Oxide Fuel Cell Anodes," *J. Fuel Cell Sci. Technol.*, vol. 3, no. 4, p. 487, 2006.

[6] S. B. Simonsen, K. Agersted, K. V. Hansen, T. Jacobsen, J. B. Wagner, T. W. Hansen, and L. T. Kuhn, "Environmental TEM study of the dynamic nanoscaled morphology of NiO/YSZ during reduction," *Appl. Catal. A Gen.*, vol. 489, pp. 147–154, Jan. 2015.

[7] S. B. Simonsen, K. Agersted, K. V. Hansen, T. Jacobsen, J. B. Wagner, T. W. Hansen, and L. T. Kuhn, "NiO/YSZ Reduction for SOFC/SOEC Studied In Situ by Environmental Transmission Electron Microscopy," *ECS Trans.*, vol. 64, no. 2, pp. 73–80, Sep. 2014.

[8] K. V. Hansen, T. Jacobsen, K. Thyden, Y. Wu, and M. B. Mogensen, "In situ surface reduction of a NiO-YSZ-alumina composite using scanning probe microscopy," *J. Solid State Electrochem.*, vol. 18, no. 7, pp. 1869–1878, Feb. 2014.

[9] D. Vladikova, Z. Stoynov, Z. Wuillemin, D. Montinaro, P. Piccardo, I. Genov, and M. Rolland, "Impedance Studies of the Reduction Process in NiO-YSZ SOFC Anodes," *ECS Trans.*, vol. 68, no. 1, pp. 1161–1168, Jul. 2015.

[10] T. S. Li, W. G. Wang, H. Miao, T. Chen, and C. Xu, "Effect of reduction temperature on the electrochemical properties of a Ni/YSZ anode-supported solid oxide fuel cell," *J. Alloys Compd.*, vol. 495, no. 1, pp. 138–143, Apr. 2010.

[11] M. Pihlatie, A. Kaiser, P. H. Larsen, and M. Mogensen, "Dimensional Behaviour of Ni-YSZ Anode Supports for SOFC Under RedOx Cycling Conditions," *ECS Trans.*, vol. 7, no. 1, pp. 1501–1510, 2007.

[12] A. Faes, A. Hessler-Wyser, A. Zryd, and J. Van herle, "A Review of RedOx Cycling of Solid Oxide Fuel Cells Anode," *Membranes (Basel).*, vol. 2, no. 4, pp. 585–664, Aug.

2012.

[13] C.-K. Lin, T.-T. Chen, A.-S. Chen, Y.-P. Chyou, and L.-K. Chiang, “Finite Element Analysis of Thermal Stress Distribution in Planar SOFC,” in *ECS Transactions*, 2007, vol. 7, no. 1, pp. 1977–1986.

[14] A. Nakajo, F. Mueller, J. Brouwer, J. Van herle, and D. Favrat, “Mechanical reliability and durability of SOFC stacks. Part I : Modelling of the effect of operating conditions and design alternatives on the reliability,” *Int. J. Hydrogen Energy*, vol. 37, no. 11, pp. 9249–9268, Jun. 2012.

[15] H. L. Frandsen, M. Makowska, F. Greco, C. Chatzichristodoulou, D. W. Ni, D. J. Curran, M. Strobl, L. T. Kuhn, and P. V. Hendriksen, “Accelerated creep in solid oxide fuel cell anode supports during reduction,” *J. Power Sources*, vol. 323, pp. 78–89, Aug. 2016.

[16] A. C. Tomkiewicz, M. A. Tamimi, A. Huq, and S. McIntosh, “Structural analysis of PrBaMn2O5+δ under SOFC anode conditions by in-situ neutron powder diffraction,” *J. Power Sources*, vol. 330, pp. 240–245, 2016.

[17] K. An, B. Clausen, A. D. Stoica, B. L. Armstrong, H. D. Skorpenske, and X.-L. Wang, “In-situ neutron diffraction study of phase stress evolutions in a Ni-based porous anode solid oxide fuel cells under uniaxial load,” *Appl. Phys. A*, vol. 99, no. 3, pp. 579–584, Apr. 2010.

[18] M. Strobl, I. Manke, N. Kardjilov, a Hilger, M. Dawson, and J. Banhart, “Advances in neutron radiography and tomography,” *J. Phys. D. Appl. Phys.*, vol. 42, no. 24, p. 243001, Dec. 2009.

[19] W. Kockelmann, G. Frei, E. H. Lehmann, P. Vontobel, and J. R. Santisteban, “Energy-selective neutron transmission imaging at a pulsed source,” *Nucl. Instruments Methods Phys. Res. Sect. A Accel. Spectrometers, Detect. Assoc. Equip.*, vol. 578, no. 2, pp. 421–434, Aug. 2007.

[20] J. R. Santisteban, L. Edwards, and V. Stelmukh, “Characterization of textured materials by TOF transmission,” *Phys. B Condens. Matter*, vol. 385–386, pp. 636–638, Nov. 2006.

[21] N. Kardjilov, I. Manke, A. Hilger, S. Williams, M. Strobl, R. Woracek, M. Boin, E. Lehmann, D. Penumadu, and J. Banhart, “Neutron Bragg-edge mapping of weld seams,” *Int. J. Mater. Res. (formerly Zeitschrift fuer Met.*, vol. 103, no. 2, pp. 151–154, Feb. 2012.

[22] R. Woracek, D. Penumadu, N. Kardjilov, A. Hilger, M. Boin, J. Banhart, and I. Manke, “3D mapping of crystallographic phase distribution using energy-selective neutron tomography.,” *Adv. Mater.*, vol. 26, no. 24, pp. 4069–73, Jun. 2014.

[23] A. S. Tremsin, J. B. McPhate, W. Kockelmann, J. V. Vallerga, O. H. W. Siegmund, and W. B. Feller, “High resolution Bragg edge transmission spectroscopy at pulsed neutron sources: Proof of principle experiments with a neutron counting MCP detector,” *Nucl. Instruments Methods Phys. Res. Sect. A Accel. Spectrometers, Detect. Assoc. Equip.*, vol. 633, no. April 2008, pp. S235–S238, May 2011.

[24] M. Strobl, R. Woracek, N. Kardjilov, A. Hilger, R. Wimpory, A. Tremsin, T. Wilpert, C. Schulz, I. Manke, and D. Penumadu, “Time-of-flight neutron imaging for spatially resolved strain investigations based on Bragg edge transmission at a reactor source,” *Nucl. Instruments Methods Phys. Res. Sect. A Accel. Spectrometers, Detect. Assoc. Equip.*, vol. 680, pp. 27–34, Jul. 2012.

[25] J. R. Santisteban, L. Edwards, a. Steuwer, and P. J. Withers, “Time-of-flight neutron transmission diffraction,” *J. Appl. Crystallogr.*, vol. 34, no. 3, pp. 289–297, May 2001.

[26] M. G. Makowska, M. Strobl, E. M. Lauridsen, H. L. Frandsen, A. S. Tremsin, T. Shinohara, and L. Theil Kuhn, “Phase Transition Mapping by Means of Neutron Imaging in SOFC Anode Supports During Reduction Under Applied Stress,” *ECS Trans.*, vol. 68, no. 1, pp. 1103–1114, 2015.

[27] M. G. Makowska, “In-situ Neutron Imaging of Solid Oxide Fuel Cells Energy resolved neutron imaging of NiO-YSZ under redox cycling,” Technical University of Denmark, 2016.

[28] M. G. Makowska, L. Theil Kuhn, L. N. Cleemann, E. M. Lauridsen, H. Z. Bilheux, J. J. Molaison, L. J. Santodonato, A. S. Tremsin, M. Grosse, M. Morgano, S. Kabra, and M. Strobl, “Flexible sample environment for high resolution neutron imaging at high temperatures in controlled atmosphere,” *Rev. Sci. Instrum.*, vol. 86, no. 12, p. 125109, Dec. 2015.

[29] M. Morgano, S. Peetermans, E. H. Lehmann, T. Panzner, and U. Filges, “Neutron imaging options at the BOA beamline at Paul Scherrer Institut,” *Nucl. Instruments Methods Phys. Res. Sect. A Accel. Spectrometers, Detect. Assoc. Equip.*, vol. 754, pp. 46–56, Aug. 2014.

[30] S. H. Williams, a Hilger, N. Kardjilov, I. Manke, M. Strobl, P. a Douissard, T. Martin, H. Riesemeier, and J. Banhart, “Detection system for microimaging with neutrons,” *J. Instrum.*, vol. 7, no. 2, pp. P02014–P02014, Feb. 2012.

[31] C. Tötzke, I. Manke, A. Hilger, G. Choinka, N. Kardjilov, T. Arlt, H. Markötter, A. Schröder, K. Wippermann, D. Stolten, C. Hartnig, P. Krüger, R. Kuhn, and J. Banhart, “Large area high resolution neutron imaging detector for fuel cell research,” *J. Power Sources*, vol. 196, no. 10, pp. 4631–4637, May 2011.

[32] W. Treimer, M. Strobl, N. Kardjilov, A. Hilger, and I. Manke, “Wavelength tunable device for neutron radiography and tomography,” *Appl. Phys. Lett.*, vol. 89, no. 20, p. 203504, Nov. 2006.

[33] M. G. Makowska, L. Theil Kuhn, E. M. Lauridsen, H. L. Frandsen, S. Kabra, W. Kockelmann, A. S. Tremsin, and M. Strobl, “In-situ time-of-flight neutron imaging studies of NiO-YSZ reduction under influence of stress.,” *Submitt. to J. Appl. Crystallogr.*

[34] R. Allen, T. Stephenson, C. Stanford, and S. Bernstein, “Slow Neutron Cross Sections of Gold, Silver, Indium, Nickel, and Nickel Oxide,” *Phys. Rev.*, vol. 15, no. 5, pp. 1297–1305, 1954.

[35] M. G. Makowska, M. Strobl, E. M. Lauridsen, H. L. Frandsen, A. S. Tremsin, N. Kardjilov, I. Manke, J. F. Kelleher, and L. Theil Kuhn, “Effect of stress on NiO reduction in solid oxide fuel cells: a new application of energy-resolved neutron imaging,” *J. Appl. Crystallogr.*, vol. 48, pp. 401–408, 2015.